Appl. Phys. A 69, 149–153 (1999) / Digital Object Identifier (DOI) 10.1007/s003399900063

Applied Physics A
Materials
Science & Processing

Electronic behaviour of thin-film CdTe solar cells

M. Burgelman, P. Nollet, S. Degrave

Universiteit Gent, Electronics and Information Systems (ELIS), Pietersnieuwstraat 41, B-9000 Gent, Belgium
(Fax: +32-9/264-3594, E-mail: Burgelman@elis.rug.ac.be)

Received: 1 March 1999/Accepted: 28 March 1999/Published online: 1 July 1999

Abstract. New support is given for one of the controversial models about the electronic consequences of the $CdCl_2$ treatment of a thin-film CdTe solar cell: the assumption that deep acceptor states are introduced in the bulk of the CdTe layer as a result of the $CdCl_2$ treatment. A detailed study of the doping profile using capacitance–voltage ($C-V$) measurements is performed as a first step. The above assumption is numerically simulated with our simulation programme SCAPS. In this way, anomalous features of the $C-V$ measurements are fully explained, and further correspondence between calculated and measurable quantities is found.

PACS: 73.50.Pz; 73.61.Ga; 78.66.Hf

Thin-film CdTe solar cells are now being developed for large-scale production [1–3]. However, their internal electronic structure is complicated and still needs further understanding. To this purpose, two features of the CdTe solar cell are intensely studied: the back contact to the CdTe film, and the treatment of the CdTe film with $CdCl_2$. Roll-over of the current–voltage ($I-V$) characteristics is by now reasonably well understood and explained in terms of a blocking diode at the back contact [4, 5]. Some phenomena accompanying roll-over, such as cross-over and the occurrence of extrema in the capacitance–voltage ($C-V$) measurements are explained in qualitative terms [6]. Considerable work has been done on the changes provoked by the $CdCl_2$ treatment to the crystallographic structure, the morphology, the composition, the defect chemistry of the CdTe films [for example 7–10], and on the changes to the solar cell characteristics J_{sc}, V_{oc}, FF and η [for example 11–13]. However, the explanation of the electronic effects of the $CdCl_2$ treatment is still controversial [10, 14].

In this paper, we will start from some basic ac measurements, and we will show that the classical $C-V$ analysis fails. To remedy the shortcomings of the classical analysis, numerical modelling is needed. The results of such numerical analysis will be used in a semi-quantitative explanation of the most striking features of the electronic properties of the back contact, and of the electronic consequences of the $CdCl_2$ treatment.

1 Experimental

Thin-film CdTe solar cells were fabricated by Antec GmbH, using CSS to deposit CdS and CdTe [1, 14]. The substrate was SnO_2-coated glass, and the back contact consisted of evaporated gold dots. Admittance measurements were carried out with a Hewlett-Packard HP4192A LCR bridge, and $I-V$ measurements with a Keithley SMU236. The measuring temperature was varied between 100 K and 350 K (AirLiquide/Eurotherm cryostat set-up).

2 $C-V$ analysis

$C-V$ measurements at forward bias voltage and for various measuring frequencies are shown in Fig. 1 (untreated cell), and in Fig. 2 (cell treated with $CdCl_2$). The main features of these curves were already explained in earlier work [5, 6]: The ac-circuit representation of the CdTe/CdS solar cell junction and of the CdTe/back contact junction is a capacitor in parallel with a conductor; both circuits are placed in series with each other. At low voltages ($V < 0.3$ V), the cell junction is limiting the current, and hence the cell junction capacitance C_j is measured. At high voltages ($V > 0.6$ V), and at low frequencies, the contact junction is limiting the current (causing roll-over), and the contact capacitance C_c is measured. At intermediate voltages, both capacitances determine

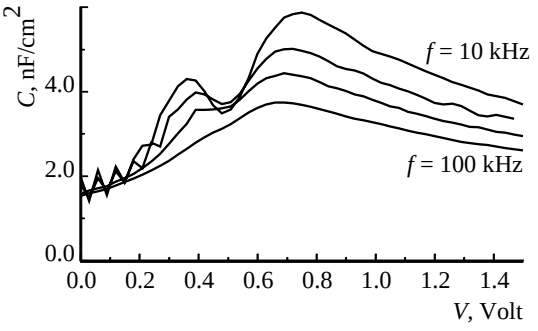

Fig. 1. Measured $C-V$ characteristics at forward bias voltage for an untreated cell; at various frequencies (10 kHz, 20 kHz, 40 kHz, and 100 kHz)

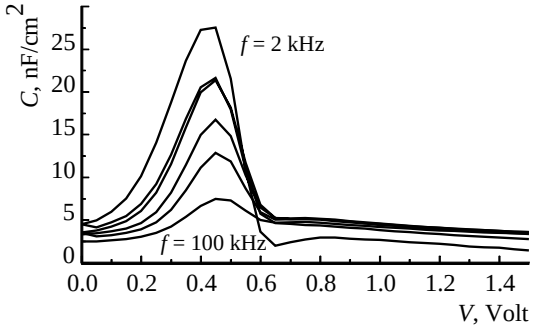

Fig. 2. Measured $C-V$ characteristics at forward bias voltage for a $CdCl_2$-treated cell; at various frequencies (2 kHz, 4 kHz, 10 kHz, 20 kHz, 40 kHz, and 100 kHz)

the ac behaviour and their series connection C_{series} ($< C_{\text{j}}$, C_{c}) is measured: this causes the minimum between two maxima in the $C-V$ measurement.

It follows that one can apply the classical $1/C^2-V$ analysis at negative and moderately positive bias voltage, to determine the acceptor density N_{Aj} in the CdTe layer near the solar cell junction. At high positive bias, the acceptor density N_{Ac} in the CdTe layer near the back contact is probed (Fig. 3). In both the treated and the untreated cell (Figs. 1 and 2), the CdTe layer is rather highly doped in the contact region: $N_{\text{Ac}} \cong 2\times10^{14}\,\text{cm}^{-3}$, up to a distance of at least 3 μm into the CdTe. In the cell junction region, the doping density is lower: $N_{\text{Aj}} \cong 1.6\times10^{13}\,\text{cm}^{-3}$ for the untreated cell, and $N_{\text{Aj}} \cong 3.2\times10^{13}\,\text{cm}^{-3}$ for the treated cell of Fig. 2. When N_{Aj} is measured at increasing negative bias voltage, thus at increasing distance from the junction, it increases, and gradually approaches N_{Ac}.

The application of the $1/C^2-V$ analysis to the junction region ($V<0.3\,\text{V}$) results in a very low value of the built-in voltage V_{bi}: 214 mV in the case of Fig. 3. The distance between the valence band and the Fermi level is calculated to be $\eta_{\text{p}}=390\,\text{mV}$ (with $N_{\text{Aj}}=1.6\times10^{13}\,\text{cm}^{-3}$ and $N_{\text{V}}=7.6\times10^{18}\text{cm}^{-3}$), so the expected value of the built-in voltage is: $V_{\text{bi}}=E_{\text{g}}-\eta_{\text{p}}-\Delta E_{\text{C}}=1.06\,\text{eV}-\Delta E_{\text{C}}$. An unrealistically high value of the conduction band discontinuity ΔE_{C} has to be assumed to explain the observed value of V_{bi}.

A possible explanation for the low apparent V_{bi} is the assumption that the effective doping density increases towards the junction. If this increase were stepwise, thus if

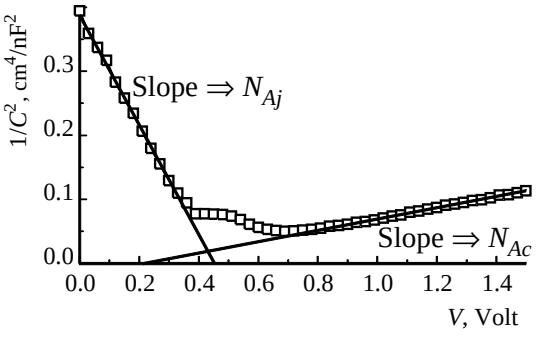

Fig. 3. $1/C^2-V$ plot for the untreated cell of Fig. 1, measured at $f=$ 40 kHz. Determination of acceptor densities N_{Ac} and N_{Aj} and the built-in voltages V_{bi} (both for the junction and the blocking contact)

$N_{\text{A}}(x)=N_{\text{A1}}$ for $x<L$ and $N_{\text{A}}(x)=N_{\text{A2}}$ for $x>L$, with $N_{\text{A1}}>N_{\text{A2}}$, the apparent V_{bi} is easily calculated as:

$$V_{\text{bi,apparent}}=V_{\text{bi}}-\frac{q(N_{\text{A1}}-N_{\text{A2}})L^2}{2\varepsilon_{\text{s}}\varepsilon_0}\,. \qquad (1)$$

The $1/C^2-V$ plot of such a simplified case is shown in Fig. 4, explaining (1).

Doping profiles $N_{\text{A}}(W)$ are deduced from the $1/C^2-V$ plots, and shown in Fig. 5 for the untreated cell, and in Fig. 6 for the cell treated with $CdCl_2$. The low voltage range $0\,\text{V}<V<0.3\,\text{V}$ is used to characterise the junction region; the depletion width $W=\varepsilon_{\text{s}}\varepsilon_0/C$ is then the distance to the junction (at $x=9.9$ μm). Attempts to probe the CdTe doping level closer to the junction by analysing the $C-V$ curve at a higher positive bias, fail since the $C-V$ curve is increasingly dominated by the contact capacitance C_{c}. The high-voltage region $V>0.7\,\text{V}$ is used to characterise the contact region; the depletion width W is then the distance to the contact (at $x=0$). Figures 5 and 6 also show calculated values of the charge density $\rho(x)$; this will be discussed later. The measurements tend to support the assumption of a steep increase in doping density towards the junction.

An obvious reason for such increase could be diffusion of species from the CdS layer. Indeed, interdiffusion of S and Te between CdS and CdTe at high processing temperatures is

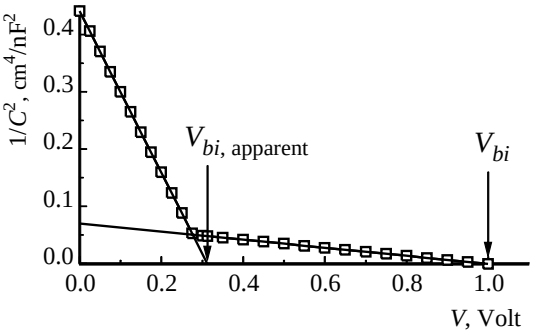

Fig. 4. $1/C^2-V$ plot for a stepped doping profile as a possible explanation for the low apparent value of V_{bi}

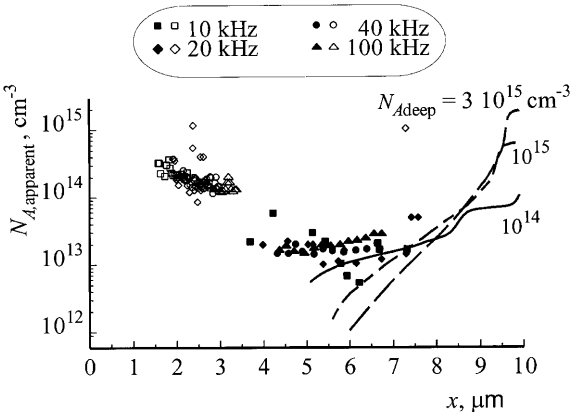

Fig. 5. Apparent doping profile for the untreated cell, from a $1/C^2-V$ analysis of the data of Fig. 1. The *points* are for the frequencies 10, 20, 40, and 100 kHz. *Open symbols* are for the contact region, and closed symbols for the junction region. The charge density $\rho(x)$ calculated by SCAPS is shown in lines for comparison

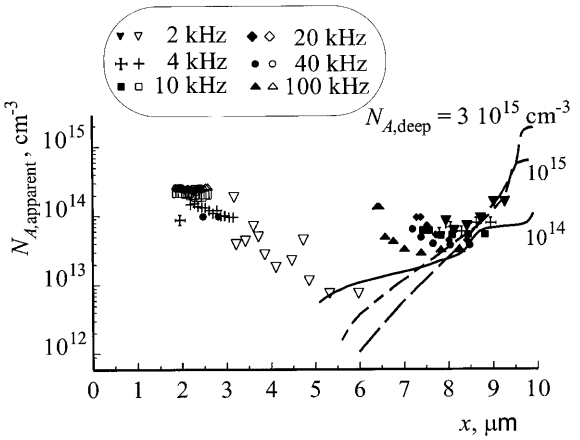

Fig. 6. Apparent doping profile for the $CdCl_2$-treated cell, from a $1/C^2 - V$ analysis of the data of Fig. 2. The *points* are for the frequencies 2, 4, 10, 20, 40, and 100 kHz. *Open symbols* are for the contact region, and closed symbols for the junction region. The charge density $\rho(x)$ calculated by SCAPS is shown in lines for comparison

a recognised phenomenon [15, 16]. If the $N_A(x)$ profile were caused by diffusion from CdS, the profile would be smeared out further during the $CdCl_2$ treatment. However, comparing Figs. 5 and 6, one sees that the $N_A(x)$ profile tends to become steeper upon $CdCl_2$ treatment. Hence we reject interdiffusion as the cause of the $N_A(x)$ profile. In the next section we will propose a model for the physical origin of this $N_A(x)$ profile.

3 Numerical modelling

In previous work we assumed that deep acceptor states are introduced in the bulk of the CdTe layer as a result of the $CdCl_2$ treatment [14]. By carrying out numerical calculations implementing this assumption, we could explain the evolution of the frequency dispersion of the capacitance ($C - f$ curves), and of the spectral response $Q(\lambda)$ upon $CdCl_2$ treatment. We used the simulation programme SCAPS (a Solar Cell CAPacitance Simulator) developed at our lab [5, 17, 18]. We will use here the same assumptions and parameter set as in [14] to explain the apparent increase of $N_A(x)$ towards the junction.

Two CdTe layers are assumed, one next to the contact and the other next to the junction. The materials parameters assumed for numerical input in SCAPS are listed in Table 1. At the back contact, a contact barrier of 0.43 eV relative to the Fermi level is assumed. In all layers the materials parameters are assumed to be uniform, i.e. not dependent on position. The deep acceptor states $N_{A,deep}$ are assumed to be uniformly distributed in energy, in a band between 0.4 and 1.0 eV above the valence band edge. We assume that an untreated cell has a low concentration of such states, $N_{A,deep} = 10^{14}$ cm^{-3}eV^{-1}, and that $CdCl_2$ treated cells have a higher $N_{A,deep} = 1$ to 3×10^{15} cm^{-3}eV^{-1}.

The energy band diagrams calculated in the dark and at a forward voltage of 0.3 V are shown in Fig. 7a (untreated cell) and Fig. 7b (treated cell). The deep acceptor states are occupied with electrons when they are situated beneath the hole Fermi level (in those regions where $p \gg n$), or beneath the electron Fermi level (in those regions where $p \ll n$). In Fig. 7, the position of the deep states with occupation probability $f = 1/2$ is drawn, and the position of the charged states is hatched.

In the space-charge region, the total charge $\rho(x)$ consists of the uniform shallow acceptor density and the position dependent charged deep acceptor density. The value of $\rho(x)$ is calculated with SCAPS and plotted in Figs. 5 and 6. It is clear that the calculated charge density increases towards the junction, and that this increase is steeper in the treated cell. Also the measured $N_A(x)$ points follow, at least qualitatively, this trend: the $N_A(x)$ points of the untreated cell (Fig. 5) tend to follow the calculated $\rho(x)$ value for the lowest concentration of deep acceptor states, whereas the $N_A(x)$ points of the $CdCl_2$ treated cell tend to follow the calculated $\rho(x)$ value for the highest concentration of deep acceptor states. Also the frequency dependency of the measured $N_A(x)$ points confirms our hypothesis that deep acceptors are introduced during the $CdCl_2$ treatment: It is known [19] that deep states only contribute to the measured capacitance if they are situated at the Fermi level (or, in non-equilibrium, if they are situated at the energy level where dc-occupation $f = 1/2$). At the edge of the space-charge region (SCL), this level is closer to the valence band than in the middle of the SCL, and hence the deep states, which contribute to the capacitance, are faster at the edge of the SCL than in the middle. Therefore, a lower measuring frequency is needed to probe the $N_A(x)$ concentration in the middle of the SCL; this trend is confirmed qualitatively in Figs. 5 and 6.

Table 1. SCAPS simulation parameters. In the CdTe layer next to the contact, the hole mobility is 3 cm^2/Vs for the untreated sample and 30 cm^2/Vs for the treated sample

Layer	CdTe (contact)	CdTe (junction)	CdS
Thickness /μm	3	6.9	0.1
E_g /eV	1.45	1.45	2.45
$q\chi$ /eV	4.3	4.3	4.5
N_C /cm^{-3}	1.3×10^{18}	1.3×10^{18}	1.5×10^{18}
N_V /cm^{-3}	7.6×10^{18}	7.6×10^{18}	1.8×10^{19}
μ_n /cm^2/Vs	50	50	50
μ_p /cm^2/Vs	3/30	30	20
Shallow doping / cm^{-3}	2×10^{14} (p)	10^{13} (p)	10^{17} (n)
Deep doping		10^{14} to 3×10^{15} cm^{-3} (p) 0.4 to 1 eV above E_V $\sigma_n = \sigma_p = 10^{-14}$ cm^2	
Recombination		10^{13} cm^{-3} mid gap $\sigma_n = \sigma_p = 10^{-11}$ cm^2	10^{14} cm^{-3} mid gap $\sigma_n = 10^{-11}$ cm^2 $\sigma_p = 10^{-14}$ cm^2

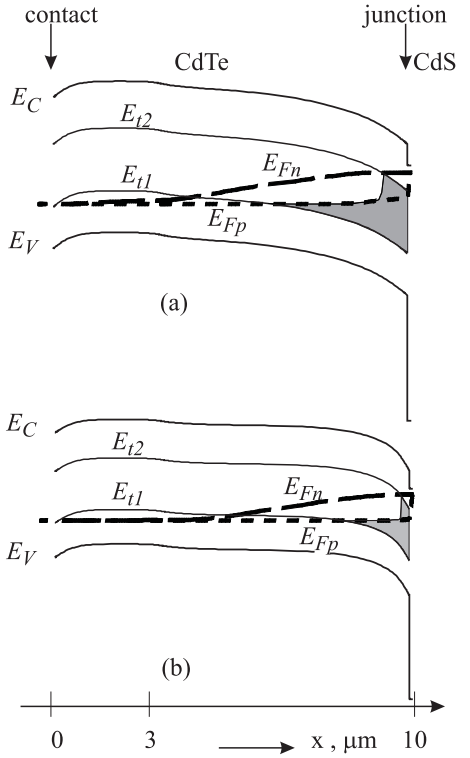

Fig. 7a,b. Calculated energy band diagram in the dark and at a forward voltage of 0.3 V for the untreated cell of Fig. 1 (**a**), and for the $CdCl_2$-treated cell of Fig. 2 (**b**)

Our assumption that the $CdCl_2$ treatment introduces deep acceptor states in the CdTe layer is explaining the $C(V, f)$ measurements well. It also explains the increase of the spectral response after $CdCl_2$ treatment. From the energy band diagrams of Fig. 7, one can easily calculate the profile of the electric field $E(x)$ in the space-charge layer; this is done in Fig. 8. The introduction of deep acceptors upon $CdCl_2$ treatment drastically increases the maximum electric field. In this way, the collection efficiency of electrons generated in the space-charge layer is also increased. If diffusion in the SCL is neglected, this collection efficiency is determined by the ratio of the minority carrier lifetime and the transit time through the SCL. To simplify the estimation of the transit time from position x to the junction (here x is the distance to the junction), the electric field is considered to be constant at its value $E(x)$, and hence:

$$Q(x) = 1 - \exp\left(-\frac{\mu\tau|E(x)|}{x}\right) . \qquad (2)$$

This is an underestimation of the real transit time and of $Q(x)$. The drift collection efficiency was calculated by inserting the $E(x)$ values calculated by SCAPS (Fig. 8) into (2); this is shown in Fig. 9. The increase of spectral response is thus to be ascribed to the following mechanism: the $CdCl_2$ treatment introduces deep acceptors, which increase the electric field in the SCL, which in turn causes a better collection efficiency in the SCL.

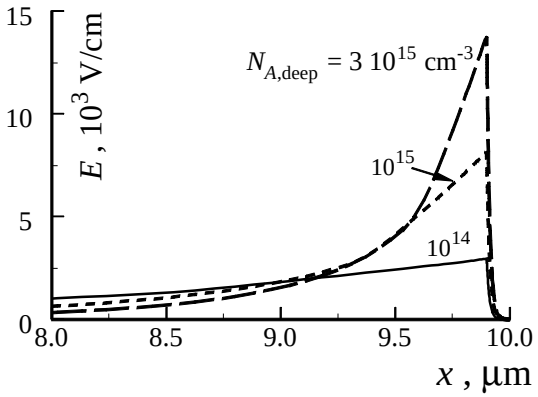

Fig. 8. Electric field $E(x)$ in the space-charge region, calculated with SCAPS

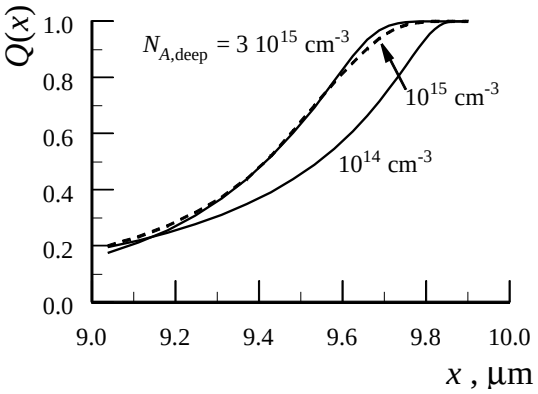

Fig. 9. Drift collection efficiency $Q(x)$ in the space-charge region, calculated from (2). The CdTe/CdS junction is at $x = 9.9$ μm

4 Conclusions

$C - V$ analysis of thin-film CdTe solar cells indicates that the apparent doping density $N_A(x)$ increases towards the junction. The influence of the $CdCl_2$ treatment on this doping profile cannot be explained by interdiffusion of species. The assumption that the $CdCl_2$ treatment introduces deep acceptor states, was formulated by us in earlier work. This work brings further corroboration to this assumption by explaining the apparent $N_A(x)$ profile and its frequency dependence, by explaining the anomalous low value of V_{bi}, and by explaining the improvement of the (drift) collection efficiency upon $CdCl_2$ treatment. The nature of the deep states, however, is not revealed by this work.

Acknowledgements. We are indebted to the Flemish Fund for Scientific Research (FWO Vlaanderen).

References

1. D. Bonnet, H. Richter, K.-H. Jäger: In Proc 13th Europ. Photovolt. Solar Energy Conf., ed. by W. Freiesleben, W. Palz, H.A. Ossenbrink, P. Helm (H.S. Stephens, Bedford, UK 1995) p. 1456
2. D. Bonnet: In Proc. 2nd World Conf. Photovolt. Solar Energy Conv., ed. by J. Schmid, H.A. Ossenbrink, P. Helm, H. Ehmann, E.D. Dunlop (European Commission, Ispra, Italy 1998) p. 397
3. W. Fuhs, R. Klenk: In Proc. 2nd World Conf. Photovolt. Solar Energy Conv., ed. by J. Schmid, H.A. Ossenbrink, P. Helm, H. Ehmann, E.D. Dunlop (European Commission, Ispra, Italy 1998) p. 381

4. G. Stollwerck, J.R. Sites: In Proc 13th Europ. Photovolt. Solar Energy Conf., ed. by W. Freiesleben, W. Palz, H.A. Ossenbrink, P. Helm (H.S. Stephens, Bedford, UK 1995) p. 2020
5. A. Niemegeers, M. Burgelman: In Proc. 25th IEEE Photovolt. Specialists Conf. (IEEE, Priscataway 1996) p. 901
6. A. Niemegeers, M. Burgelman: J. Appl. Phys. **81**, 2881 (1997)
7. N. Romeo, A. Bosio, V. Canevari: Int. J. Solar Energy **12**, 183 (1993)
8. M. Al-Jassim, F. Hasoon, K. Jones, B. Keyes, R. Matson, H. Moutinho: In Proc. 23th IEEE Photovolt. Specialists Conf. (IEEE, Priscataway 1993) p. 459
9. R. Birkmire, P.V. Meyers: In Proc. 1st World Conf. Photovolt. Solar Energy Conv. (IEEE, Priscataway 1994) p. 76
10. S.A. Ringel, A. Smith, M. MacDougal, A. Rohatgi: J. Appl. Phys. **70-2**, 881 (1991)
11. H.R. Moutinho, R. Ahmed-Bitar, F. Hasoon, R. Ahrenkiel, D. Dunlavy, B. Keyes, A. Mason, F. Abou-Elfotouh, R. Birkmire, L. Kazmerski: In Proc 11th Europ. Photovolt. Solar Energy Conf., ed. by L. Guimarães, W. Palz, C. De Reyff, H. Kiessand, P. Helm (Harwood, Chur, Switzerland 1992) p. 991
12. D. Bonnet, B. Henrichs, H. Richter: Int. J. Solar Energy **12**, 133 (1993)
13. Y. Loginov, K. Durose, H. Al-Allak, S. Galloway, S. Oktik, A. Brinkman, H. Richter, D. Bonnet: J. Crystal Growth. **163**, 159 (1995)
14. A. Niemegeers, M. Burgelman, H. Richter, D. Bonnet: In Proc. of the 14th Europ. Photovolt. Solar Energy Conf., ed. by H.A. Ossenbrink, P. Helm, H. Ehmann (H.S. Stephens, Bedford, UK 1995) p. 2079
15. I. Clemminck, M. Burgelman, M. Casteleyn, J. De Poorter, A. Vervaet: In Proc. 22th IEEE Photovolt. Specialists Conf. (IEEE, Priscataway 1992) p. 1114
16. I. Clemminck, M. Burgelman, M. Casteleyn, B. Depuydt: Int. J. Solar Energy **12**, 67 (1992)
17. A. Niemegeers, S. Gillis, M. Burgelman: In Proc. 2nd World Conf. Photovolt. Solar Energy Conv., ed. by J. Schmid, H.A. Ossenbrink, P. Helm, H. Ehmann, E.D. Dunlop (European Commission, Ispra, Italy 1998) p. 672
18. A. Niemegeers, S. Gillis, M. Burgelman: In Proc. 2nd World Conf. Photovolt. Solar Energy Conv., ed. by J. Schmid, H.A. Ossenbrink, P. Helm, H. Ehmann, E.D. Dunlop (European Commission, Ispra, Italy 1998) p. 1071
19. S.M. Sze: *Physics of Semiconductor Devices*, 2nd edn. (Wiley, New York 1981)